

## Research



**Cite this article:** Farr O, Gaudu N, Danger G, Russell MJ, Ferry D, Nitschke W, Duval S. 2023 Methanol on the rocks: green rust transformation promotes the oxidation of methane. *J. R. Soc. Interface* **20**: 20230386. <https://doi.org/10.1098/rsif.2023.0386>

Received: 7 July 2023

Accepted: 30 August 2023

**Subject Category:**

Life Sciences—Chemistry interface

**Subject Areas:**

biogeochemistry, environmental science, astrobiology

**Keywords:**

methane oxidation, green rust, origin of life, geochemistry, carbon cycle, Archean redox

**Author for correspondence:**

Orion Farr

e-mail: [orionfarr@gmail.com](mailto:orionfarr@gmail.com)

Electronic supplementary material is available online at <https://doi.org/10.6084/m9.figshare.c.6825590>.

# Methanol on the rocks: green rust transformation promotes the oxidation of methane

Orion Farr<sup>1,2</sup>, Nil Gaudu<sup>2</sup>, Gregoire Danger<sup>3</sup>, Michael J. Russell<sup>4</sup>, Daniel Ferry<sup>1</sup>, Wolfgang Nitschke<sup>2</sup> and Simon Duval<sup>2</sup>

<sup>1</sup>CNRS, CiNaM, Aix-Marseille Univ, 13009 Marseille, France

<sup>2</sup>CNRS, BIP (UMR 7281), Aix Marseille Univ, Marseille, France

<sup>3</sup>CNRS, PiiM, Aix-Marseille Univ, 13013 Marseille, France

<sup>4</sup>Dipartimento di Chimica, Università degli Studi di Torino, Italy

OF, 0000-0003-0478-794X; DF, 0000-0003-1469-9871; WN, 0000-0003-2084-3032; SD, 0000-0003-2946-6771

Shared coordination geometries between metal ions within reactive minerals and enzymatic metal cofactors hints at mechanistic and possibly evolutionary homology between particular abiotic chemical mineralogies and biological metabolism. The octahedral coordination of reactive Fe<sup>2+/3+</sup> minerals such as green rusts, endemic to anoxic sediments and the early Earth's oceans, mirrors the di-iron reaction centre of soluble methane monooxygenase (sMMO), responsible for methane oxidation in methanotrophy. We show that methane oxidation occurs in tandem with the oxidation of green rust to lepidocrocite and magnetite, mimicking radical-mediated methane oxidation found in sMMO to yield not only methanol but also halogenated hydrocarbons in the presence of seawater. This naturally occurring geochemical pathway for CH<sub>4</sub> oxidation elucidates a previously unidentified carbon cycling mechanism in modern and ancient environments and reveals clues into mineral-mediated reactions in the synthesis of organic compounds necessary for the emergence of life.

## 1. Introduction

Methane (CH<sub>4</sub>), although currently present at only 1.9 ppm, is the major heat-trapping greenhouse gas in terms of its radiative forcing effect, having 80× the effect of CO<sub>2</sub> [1]. Anthropogenic emissions of CH<sub>4</sub> now outweigh natural sources produced via biotic (organic degradation) and abiotic (serpentinization, mantle degassing) mechanisms. Natural sinks exist for CH<sub>4</sub> but are insufficient to offset growing anthropogenic output. In the biosphere, CH<sub>4</sub> is readily oxidized by methanotrophs, yielding methanol (MeOH), a key metabolic intermediate towards biomass formation [2,3]. In many species, this metabolism employs the enzyme soluble methane monooxygenase (sMMO) to react CH<sub>4</sub> with oxygen (O<sub>2</sub>), N<sub>2</sub>O or H<sub>2</sub>O<sub>2</sub> over an ephemeral di-Fe(IV) intermediate reaction centre to achieve the conversion of CH<sub>4</sub> to MeOH [4]. A similar reaction mechanism takes place within man-made catalysts where Fe(IV) reaction centres embedded within mineral scaffolds are used to convert CH<sub>4</sub> to value-added products [5–7]. The oxidation state Fe(IV), which is only ephemeral in nature, is crucial to the energetically demanding partial oxidation of CH<sub>4</sub> for biological and industrial purposes [7,8].

Methane is thought to have had an even larger role in climate regulation during the Hadean–Archean Eons 4.4 to 3.2 Ga, where the estimated atmospheric abundances of greenhouse gases like CH<sub>4</sub>, CO<sub>2</sub> and N<sub>2</sub>O were orders of magnitude greater than modern, supplying ample CH<sub>4</sub> for the proliferation of primitive methanotrophs [9,10]. This anaerobic metabolism, along with various others, dominated the biosphere until the emergence of oxygenic photosynthesis during the great oxidation event (GOE) [11].

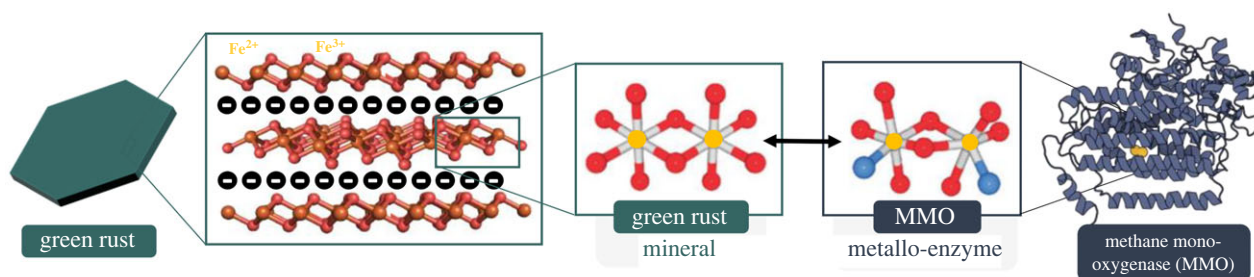


**Figure 1.** A diagram comparing the structural similarities between GR and sMMO. From left to right, an illustration of a single GR crystal, the crystal's cation and anion LDH structure, the octahedral coordination of iron (yellow) and oxygen (red) atoms in GR, the analogous atomic structure of the MMO reaction centre (nitrogen = blue) and a model of the enzyme MMO.

Of pertinence to the experiments and outcomes reported herein, the octahedral di-iron reaction centre structure of sMMO shares similar coordination geometry to the octahedral di-valent iron lattice coordination in green rusts (GRs) (figure 1) [12]. This group of naturally forming, metastable, reactive, layered double hydroxide (LDH) minerals are known for their redox capabilities in carrying out the reduction of metals (e.g. Cu, As, U), inorganic compounds (e.g.  $\text{NO}_3^-$ ,  $\text{ClO}_4^-$ ) and organic compounds (e.g. CT, TCE, TCM [13–18]). The GR unique structure consists of a charged octahedrally coordinated bilayer of di-valent  $\text{Fe}^{2+/3+}$  cations which can integrate other transition metals (e.g. Ni, Co, Zn, Mg, Al) and sandwich interchangeable anions (e.g.  $\text{CO}_3^{2-}$ ,  $\text{HCO}_3^-$ ,  $\text{Cl}^-$ ,  $\text{SO}_4^{2-}$ ) [19]. The mineral reacts with oxygen, radicals, and temperature to undergo pH- and redox-dependent transformations into other reactive minerals, namely magnetite and lepidocrocite, playing a yet unquantified role in the geochemical cycling of sub-oxic subsurface environments [20–22]. Of note is its proposed role in marine nutrient and metal geochemical cycling prior to the GOE at approximately 2.5 Ga [23,24], and its hypothesized suitability as an ‘abiotic enzyme’ linking geochemical proto-metabolism with the evolution of enzymatic biochemistry prior to the emergence of life [12,25–27].

The di-iron structure present in sMMO and synthetic catalysts is known to be the key site essential in the oxidation of methane. Thus, the presence of an analogous structure in GR suggests that it also has the potential to catalyse methane oxidation. In this study, we experimentally demonstrate the viability of this proposed analogous catalytic behaviour by reacting GR with  $\text{CH}_4$  and  $\text{O}_2$  to produce significant quantities of MeOH and halogenated organics. These results uncover previously unrecognized redox reactions with GR and the carbon cycle, yielding significant environmental implications to the modern and ancient Earth.

## 2. Methods

### 2.1. Mineral synthesis

Three GR species and their transformation products were synthesized following a procedure based on  $\text{GRCO}_3$  syntheses outlined in Ruby *et al.* [28] and Bocher *et al.* [29]. The main species of GR studied was a green rust intercalated with the carbonate anion ( $\text{GRCO}_3$ ) and its synthesis is described below. Synthesis for  $\text{GRSO}_4$  and  $\text{GRCl}$  is detailed in the electronic supplementary material, section S1.

A concentrated stock solution of simulated seawater (80 ml) containing 150 mM  $\text{FeCl}_2 \cdot \text{H}_2\text{O}$ , 50 mM  $\text{FeCl}_3$ , 50 mM of  $\text{MgCl}$  and 400 mM of  $\text{NaCl}$  was prepared using deoxygenated

ultra-purified water (Milli-Q) and purged with  $\text{N}_2$  gas for 30 min in a sealed 125 ml reactor vial. A solution (20 ml) of 300 mM  $\text{NaOH}$  and 30 mM  $\text{Na}_2\text{CO}_3$  was then injected into the reactor via a  $\text{N}_2$ -purged needle syringe and the mixture was gently shaken. A dark green precipitate formed which was then confirmed to be  $\text{GRCO}_3$  via powder X-ray diffraction (figure 3), which was stable indefinitely. The total Fe concentration in this stock solution was 200 mM and final pH was approximately 7.

### 2.2. Methane oxidation reactions

The pressurized reactions took place inside a 200 ml Parr autoclave reactor pressurized to 0, 1, 10, 30, 50 bar  $\text{CH}_4$  (Linde Gas 99.99%), 0–3 bar  $\text{O}_2$  (Linde), 1 bar  $\text{NO}$  (Linde Gas 5%), at 25°C. Within the reactor 20–100 ml glass vials with stirrers, butyl or screw top caps, and needle-perforated septa were used to contain the replicate mineral suspensions. These vials were then removed and stored under anoxic conditions before their headspaces were analysed using gas chromatography (GC) coupled to mass spectrometry (MS).

### 2.3. Headspace analysis

Gas chromatograph coupled to an ISQ mass spectrometer (ThermoFisher Scientific). The sampling was performed by headspace (HS) using an RSH auto-sampler (ThermoFisher Scientific). 5 ml of each sample was deposited on a 20 ml HS vial with screwtop PTFE septas. Each vial was then incubated during 6 min at 55°C under agitation. The HS sampling was performed by collecting 2 ml of the gas phase. It was then injected into the GC via an injector at 250°C, a split at  $10 \text{ ml min}^{-1}$  and a column flow of  $1.1 \text{ ml min}^{-1}$ . The column was a Stabilwax-DA from Restek (length 30 m, diameter 0.25 mm, film thickness 0.5  $\mu\text{m}$ ). Analyses were performed with the temperature gradient that starts with a 1 min isotherm at 35°C and proceeds with a gradient at  $25^\circ\text{C min}^{-1}$  up to 220°C ending with a 2 min isotherm. The detection was performed with the MS in full scan or SIM mode using an electron impact ionization at 70 eV. MS transfer line and ion source temperatures were set at 250°C. For the full-scan analyses, the  $m/z$  range was 20–300 au, meanwhile for the SIM  $m/z$  31 and 84 were isolated for MeOH and TCM identification (electronic supplementary material, figure S6).

### 2.4. Mineral characterization

Mineral transformation over the course of the reaction was monitored using X-ray diffraction (XRD), transmission electron microscopy (TEM) and scanning electron microscopy (SEM). Samples were centrifuged, decanted and dried under a stream of  $\text{N}_2$  gas. For XRD analysis, glycerol was added prior to analysis to prevent oxidation and the paste was transferred into a glass ampule for XRD analysis in a Rigaku RU 200BH diffractometer with Cu anode ( $\lambda = 1.5418 \text{ \AA}$ ), scanning at  $2\theta$  values of  $2^\circ$ – $80^\circ$ . For TEM analysis, an aliquot of dried mineral was deposited

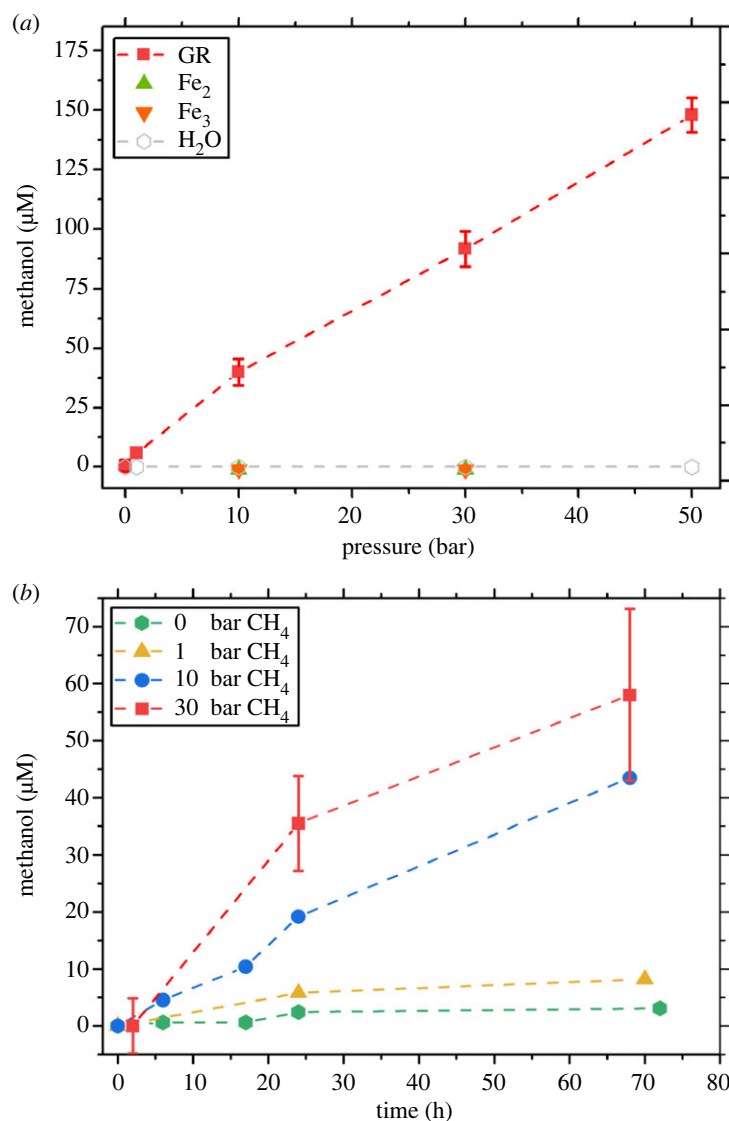


**Figure 2.** Effect of pressure and time on methanol concentration. (a) Methanol concentrations at given CH<sub>4</sub> partial pressure following 24 h of reaction time in solutions containing GRCO<sub>3</sub>, FeCl<sub>2</sub>, FeCl<sub>3</sub> and H<sub>2</sub>O. (b) A related set of experiments conducted at [Fe] = 30 mM, showing methanol production over time.

on a copper grid coated with a holey carbon film (AGAR Scientific, S147-3). Grids were then transferred to a Jeol JEM2010 electron microscope operated at 200 kV and GR particles were observed in bright field mode. For SEM analysis, an aliquot of dried mineral was deposited on an aluminium sample holder and then transferred to a Jeol JSM-7900F electron microscope and analysed using accelerating voltages ranging from 5 to 15 kV.

### 3. Results

The pressurization of GR with CH<sub>4</sub> and O<sub>2</sub> resulted in the production of MeOH along with various other compounds, including trichloromethane (TCM) and dichloromethane (DCM). Various conditions were tested to optimize the yield of MeOH.

Figure 2a shows MeOH concentrations in solutions of GRCO<sub>3</sub> ([Fe] = 200 mM) following 24 h of pressurization to 0, 1, 10, 30 and 50 bar CH<sub>4</sub> mixed with 0.2 bar O<sub>2</sub>. There is a significant increase in MeOH concentration with increasing pressure. At 10 bar CH<sub>4</sub>, solutions of GRCO<sub>3</sub> with a total [Fe] = 200 mM yield 30 μM MeOH which increases fivefold with a corresponding fivefold increase to 50 bar CH<sub>4</sub>. Thus,

MeOH concentration increases with a linear relationship with pressure ( $y = (2.88 \times 10^{-6})x + 5.30 \times 10^{-6}$ ). Multiple concentrations were examined and the relationship between [MeOH]/[Fe] is compared (electronic supplementary material, figure S5). MeOH is only detected with GR in the initial solution, as solutions containing FeCl<sub>2</sub>, FeCl<sub>3</sub> or H<sub>2</sub>O did not produce detectable levels of MeOH under the same conditions. No MeOH is detected without the added oxidants. Substitutes for O<sub>2</sub>, NO and H<sub>2</sub>O<sub>2</sub> were tested and found to produce products of CH<sub>4</sub> oxidation (electronic supplementary material, figure S7).

Figure 2b shows the production of MeOH over time in solutions of GRCO<sub>3</sub> ([Fe] = 30 mM) with partial pressures of CH<sub>4</sub> from 0 to 30 bar mixed with 0.2 bar O<sub>2</sub>. These experiments were conducted at lower concentrations of Fe than figure 2 (30 versus 200 mM). No MeOH is detected in solutions of GR not exposed to CH<sub>4</sub>. With 1 bar CH<sub>4</sub>, there is a mild increase to approximately 5 μM of MeOH. At 10 bar CH<sub>4</sub>, there is an increase from 0 to approximately 40 μM of MeOH by 80 h. At 30 bar CH<sub>4</sub>, we show an increase from 0 to approximately 55 μM of MeOH by 68 h of reaction time. The addition of 0.2 bar O<sub>2</sub> and subsequent MeOH production resulted in changes to solution pH, which was recorded to drop from an initial

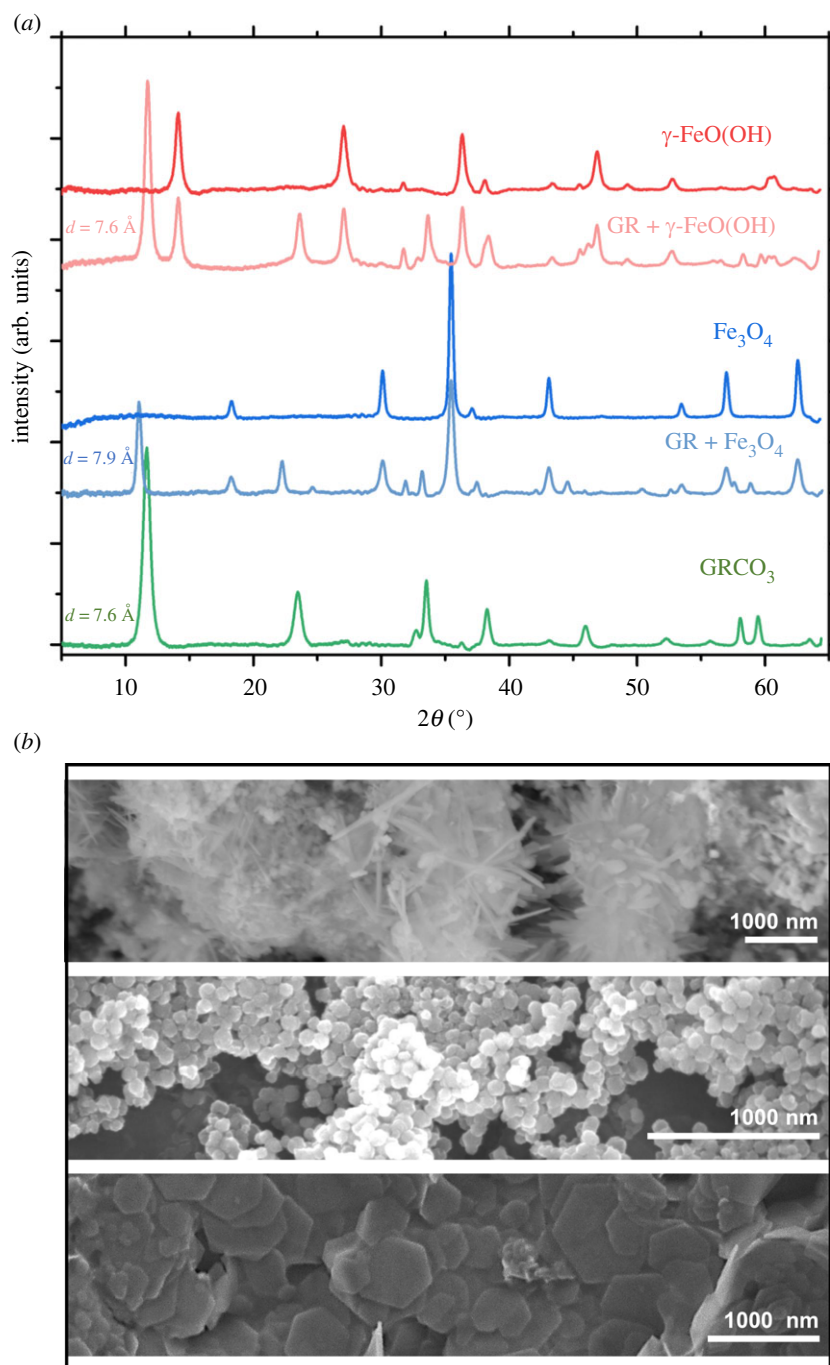


**Figure 3.** XRD and TEM of GR transformation products. (a) XRD diffractograms of the mineral species produced following the exposure of GRCO<sub>3</sub> to pressurized CH<sub>4</sub>/O<sub>2</sub> atmospheres. Magnetite (Fe<sub>3</sub>O<sub>4</sub>) and lepidocrocite (γ-FeO(OH)) were the primary transformation products of GR corresponding to low (approx. 0.1 bar) and high (greater than 0.1 bar) O<sub>2</sub> content, respectively. Partially transformed products are displayed below the primary product, with the residual GR's low 2θ d-spacing listed adjacent. (b) The corresponding SEM images of the pure mineral phases characterized in (a).

value of 7 to 6 by 24 h and 5 by approximately 70 h. Additional experiments were attempted with 1 bar O<sub>2</sub> and 10 bar CH<sub>4</sub>, leading to rapid mineral transformation yet no measurable MeOH production.

Coinciding with MeOH production was the production of various organic compounds produced in micromolar quantities. The most prevalent compounds detected other than MeOH were halogenated organics, mainly TCM and DCM (electronic supplementary material, figure S2). The concentration of TCM and DCM increased in response to increased pressure; however, DCM was the primary organo-halogen detected at higher pressures (30 bar) versus TCM dominating at lower pressures. Trace amounts of TCM were also detected without the presence of O<sub>2</sub> in aged GRCO<sub>3</sub>

solutions exposed to CH<sub>4</sub>. However, TCM was also produced in solutions of FeCl<sub>2</sub> when exposed to CH<sub>4</sub>. Other organic products were produced but were not easily replicated and thus were not quantified: these compounds included C<sub>1</sub>–C<sub>12</sub> hydrocarbons, butanal, pentanal, paraformaldehyde, acetaldehyde and dimethyl ether.

GR undergoes transformation to two mineral phases following the exposure to pressurized CH<sub>4</sub> and O<sub>2</sub> mixtures, oxidizing to either magnetite (Fe<sub>3</sub>O<sub>4</sub>) or lepidocrocite (γ-FeO(OH)) according to XRD (figure 3a). The presence of O<sub>2</sub> (0–1 bar) at the start of the reaction resulted in different transformation product yields, with increased O<sub>2</sub> selecting for γ-FeO(OH) over Fe<sub>3</sub>O<sub>4</sub>. In the case of transformation to Fe<sub>3</sub>O<sub>4</sub>, d-spacing for the low 2θ peak shifts from 7.6 to



7.9 Å. Full transformation takes place within 68 h of reaction. SEM (figure 3*b*) images show distinct transformation from GR's characteristic 10–500 nm hexagonal platelets, through an intermediate phase with hexagonal plates studded with less than 100 nm spheroid assemblages or less than 100 nm irregular acicular crystals, to a fully transformed phase with only spheroids or acicular crystals. The transformation of GR results in a decrease from an initial average pH of 7 to a pH of 5.

## 4. Discussion

Our experiments show that the oxidative transformation of GR in the presence of CH<sub>4</sub> results in the oxidation of CH<sub>4</sub>, to a variety of products. In §4.1, we discuss the analysis of MeOH, as well as the other compounds (e.g. TCM, DCM) detected in significant quantities.

### 4.1. The concurrent oxidation of green rust and methane

The production of MeOH at various pressures and over time is depicted in figure 2, showing significant quantities are produced in solutions of GR pressurized to 1–50 bar over 60 h, given the initial presence of 0.2 bar of O<sub>2</sub> at the start of the experiment. However, in the absence of oxygen, the introduction of CH<sub>4</sub> to GR resulted in little to no MeOH production. Substitutes for O<sub>2</sub> were tested, using H<sub>2</sub>O<sub>2</sub> (electronic supplementary material, figure S5) and NO (electronic supplementary material, figure S7) in separate experiments, yielding MeOH and butanal, respectively. The presence of a sufficient oxidant is therefore implicated in the successful oxidation of methane using GR.

Increasing CH<sub>4</sub> pressure resulted in a linear increase in MeOH concentration over a range of [Fe] (200, 100, 30 mM). Increasing the concentration of Fe results in higher yield of MeOH; however, the efficiency of the production of MeOH/Fe falls dramatically (electronic supplementary material, figure S5). GR's affinity to hydrophilic O<sub>2</sub> as well as radical scavenging likely dominates surface interactions versus hydrophobic gases like CH<sub>4</sub>. The reaction rate is thus dependent on how much CH<sub>4</sub> is in contact with the mineral surface, which is controlled by the concentration of dissolved CH<sub>4</sub> in solution (figure 2). CH<sub>4</sub> solubility is controlled by pressure and chloride concentration due to CH<sub>4</sub>'s low solubility in distilled water at STP (25°C; 1 bar)—solubility increases 42% from 1 to 50 bar but is decreased by 20% with the addition of 0.4 M Cl<sup>-</sup> [30]. The solubilization of CH<sub>4</sub> is one route for aqueous mineral reactions; however, within pore spaces common to sediments and hydrothermal systems where this reaction would occur, direct contact with trapped CH<sub>4</sub> bubbles would offer a more direct mineral-to-gas interface, increasing the reaction rate.

The substitution of interlayer anions is known to affect GR reactivity [31] and our investigation of Cl<sup>-</sup>, CO<sub>3</sub><sup>2-</sup>, and SO<sub>4</sub><sup>2-</sup> (electronic supplementary material, figure S4) shows an unexpected trend in reactivity with CO<sub>3</sub><sup>2-</sup> > Cl<sup>-</sup> > SO<sub>4</sub><sup>2-</sup>. With prior work in GR, redox reactions involving the various anions show clear preference for Cl<sup>-</sup> and SO<sub>4</sub><sup>2-</sup> over CO<sub>3</sub><sup>2-</sup> reactions [19]. A shift in d-spacing (figure 3) from 7.6 to 7.9 Å corresponds to a shift in interlayer anion species from CO<sub>3</sub><sup>2-</sup> to Cl<sup>-</sup> during transformation from GR to Fe<sub>3</sub>O<sub>4</sub> [19].

As the GRCO<sub>3</sub> and GRCl solutions were conducted in simulated seawater, a mixed or transitory interlayer phase of CO<sub>3</sub><sup>2-</sup> + Cl<sup>-</sup> could conceivably be responsible for increased reactivity towards CH<sub>4</sub> oxidation. The increased MeOH production could also be linked to the reduction of interlayer bound CO<sub>3</sub><sup>2-</sup> during the reaction [32].

The production of halogenated organic molecules was observed (electronic supplementary material, figure S2): GR appears to catalyse CH<sub>4</sub> chlorination as TCM and DCM are products in solutions containing GR and NaCl. GR and magnetite are known to reduce halogenated organics [33], which may explain the preference for DCM over TCM at higher pressure. Given time, this reduction should continue to methyl chloride and CH<sub>4</sub>. Chlorine could likely be replaced by other environmentally relevant halogens such as iodine or bromine, indicating a general abiotic link between Fe redox and halogen cycling in the environment.

MeOH was not detected in parallel experiments using solutions of H<sub>2</sub>O, NaCl or FeCl<sub>2</sub>, or FeCl<sub>3</sub> in place of GR. Since no MeOH is formed without GR or without O<sub>2</sub>, GR must be producing a short-lived reactant during oxidation necessary for the reaction to proceed over GR or its oxide transformation products; ferric green rust, magnetite or lepidocrocite.

### 4.2. Radicals and Fe(IV)-mediated oxidation mechanism

The presence of radicals and Fe(IV) oxidation states are routinely implicated in CH<sub>4</sub> oxidation research as a main mechanism for achieving the energetically difficult partial oxidation of methane over transition metal bearing mineral catalysts such as zeolites [6,7]. These high surface area aluminosilicate minerals bear Fe(II–III) reaction sites which readily react with oxidative species such as O<sub>2</sub>, H<sub>2</sub>O<sub>2</sub>, N<sub>2</sub>O, UV or radicals to create short-lived reactive Fe(IV) oxidation states which can effectively conduct CH<sub>4</sub> oxidation [5,7,34]. This Fe(IV) state is likewise responsible for CH<sub>4</sub> oxidation in microbial methanotrophy, where the enzyme sMMO uses oxidant-activated Fe(IV) reaction centres to transform CH<sub>4</sub> to MeOH [4]. Correspondingly, in GR, it is oxidative transformation is known to produce a significant amount of hydroxyl radicals, H<sub>2</sub>O<sub>2</sub> and Fe(IV) sites [35,36] which have been observed to promote the degradation of complex organic molecules [37,38].

Given the known relationship between radical production, Fe(IV) sites and methane oxidation, we propose that GR mediates CH<sub>4</sub> oxidation via radical-mediated oxidation pathway over short-lived Fe(IV) sites in a manner similar to sMMO [8] or Fe-ZSM zeolites [6].

To further test this hypothesis, we replicated the experimental conditions for GRCO<sub>3</sub> at 1 bar CH<sub>4</sub> and replaced O<sub>2</sub> with 1 mM of H<sub>2</sub>O<sub>2</sub> which yielded a significant amount of MeOH even without high pressures (electronic supplementary material, figure S5). This indicates the reaction is dependent on the interaction between hydroxyl radicals, iron and CH<sub>4</sub> [39]. Furthermore, MeOH serves as a radical scavenger resulting in its own oxidation to formaldehyde (which was detected), formate and CO<sub>2</sub> [40]. The production of organohalogens in the presence of Cl<sup>-</sup> anions, likely through a radical chlorination pathway [41], adds further evidence to the radical-based hypothesis. In this case, the Cl<sup>-</sup> radical ion substitutes for the hydroxyl radical to oxidize CH<sub>4</sub> yielding methyl chloride (MC), DCM and TCM, instead of MeOH, which was observed in our experiments.

### 4.3. Implications

The discovery of a naturally occurring mineral-based mechanism for CH<sub>4</sub> oxidation is novel and hints at large-scale geochemical processes that have been overlooked with past research.

#### 4.3.1. Feasibility and environmental relevance

The conditions simulated within the pressure reactor (GR in contact with pressurized CH<sub>4</sub>) provided optimal conditions for the reaction in addition to serving as an analogue to environmental conditions where GR could conceivably interact with sources of CH<sub>4</sub> at depth. GR has been isolated in deep anoxic ferruginous lakes [21] and is speculated to form at hydrothermal vents and [42] where oxygen-poor hydrothermal fluids meet cold oxygen-rich seawater. In both locales, abiotic and biotic sources of CH<sub>4</sub>, pressurized at depths (e.g. 100 m depth = 10 bar pressure), would fall within the range of conditions we tested. For environments closer to STP, such as wetland sediments, soils and ground water, our experimental results still demonstrate GR's reactivity towards CH<sub>4</sub> oxidation, albeit one accelerated by pressure. We observed both MeOH and halogenated organics at 1 bar CH<sub>4</sub>, though in low concentrations, indicating that mineral-based CH<sub>4</sub> oxidation will take place even under STP. The discovery of naturally occurring mineral-based mechanism for CH<sub>4</sub> oxidation is novel and hints at global geochemical processes that have been previously overlooked.

#### 4.3.2. Implied role of green rust in carbon and halogen cycling in modern environments

GRs are well studied for their use in the degradation of organohalogen pollutants in the environment [43–46]; however, they have never been linked to organohalogen formation via CH<sub>4</sub> oxidation. Recent observations revealed that salt plains, rainforests and soils are sources of abiotic emissions of chloromethanes [47–51]. Of note is the isotopic fractionation of some of these signatures, implying an abiotic source [50]. As mentioned previously, GR is common in these types of waterlogged environments [52] and within anoxic regions of stratified bodies of water and rivers with high iron content [21,53]. In soils, Fe is already known to halogenate decaying organic matter [47]; the direct oxidation of CH<sub>4</sub> has not yet been observed in the environment. Our experiments show that it is feasible for GR to be oxidatively transformed to reactive Fe-oxides in the presence of CH<sub>4</sub>, thus catalysing abiotic CH<sub>4</sub> oxidation and chloromethane production. As CH<sub>4</sub>, halomethane and halogen flux greatly affect climate forcing [54], uncovering the role reactive minerals play in these cycles may help constrain their input over climate change. Overall, the further study of these environments should take care to identify O<sub>2</sub>-sensitive minerals like GR, to understand the extent of their influence over the geochemical cycling of carbon and halogens.

#### 4.3.3. Methane oxidation on the ancient Earth

Abiotic CH<sub>4</sub> oxidation may have played a greater role in the deep past as long periods of ferruginous oceans characterized the Archean (4–3.5 Ga) and Proterozoic (3.5–2 Ga) eons [24,55,56]. During these periods, GRs are thought to have been abundant and likely shepherded marine geochemistry

at the interface between land, air and sea [21,24,57]. Prior to the GOE and the subsequent proliferation of O<sub>2</sub> in marine environments, geochemically generated radical species [39,58–61], thermochemical processes [22,62], natural electrochemical processes [63–65], photochemistry [23,61], nitrogen oxides [18,66] and nitrogen oxyanions [67,68], may have served as potential surrogates for the oxidation of GR and thus CH<sub>4</sub>, creating a CH<sub>4</sub> sink within the ancient Archean ocean. As O<sub>2</sub> concentrations increased following the GOE, the oxidation of GR-bearing oceans may have played a role in the drawdown of atmospheric CH<sub>4</sub> concentrations [10], impacting climate throughout the Proterozoic [69,70].

As halomethanes exert strong influences over the greenhouse effect [54], the effect of their production by a GR-saturated ocean on the Archean climate is currently unstudied. As such, the detection of exoplanet halomethane signatures may not necessarily indicate the presence of life, as was recently suggested [71]. However, as life is thought to have emerged sometime in the Late Hadean to Early Archean, the oxidation of abundant CH<sub>4</sub> [10] to more biochemically accessible compounds such as MeOH, hydrocarbons and halogenated organics may have played important roles both before and after its emergence.

More specifically, our results strengthen an emergence-of-life hypothesis that invokes a pathway for GR-mediated protocell synthesis [3,12,25,26], where hydrothermal CH<sub>4</sub> is oxidized to multi-carbon compounds within GR-saturated mineral membranes precipitated at the redox boundary between reducing alkaline vent effluent and oxidizing acidic ocean water—the type of disequilibria considered to have driven life into being [72]. Just as in the biological metabolism of methanotrophy, methane would thereby serve both as a feedstock for production of organics and as a source of a cascade of increasingly reducing electrons derived from the further oxidation of MeOH, formaldehyde, etc., as discussed in [3,63]. As pointed out previously, such entropy-decreasing processes are prerequisites for thermodynamically meaningful emergence-of-life scenarios [73]. Given the similarities between sMMO's di-iron reaction centre and GR's atomic lattice coordination, a proposed evolutionary link between minerals and enzymes is suggested [74]. Because GR has a uniquely versatile structure which allows for chemical exchange, integrating several essential metals (e.g. Co, Ni, Zn, Mo) and anionic (e.g. NO<sup>3-</sup>, formate, linear carbon chain) species, it is suggested that its reactive surfaces and bilaterally active interlayers served as sites for organic synthesis and concentration [75] at early submarine alkaline hydrothermal vents, and that these interlayers also compartmentalized and guided the free-energy converting proto-metabolic processes which led to the emergence of life [12,25,26].

## 5. Conclusion

We demonstrate that the oxidative transformation of GR in the presence of methane yields methanol, along with organohalogens and various other organic compounds. This newly discovered behaviour implies the existence of previously undetected links between iron, carbon and halogen redox cycling in modern and ancient environments mediated by reactive minerals. Furthermore, the oxidation of CH<sub>4</sub> mediated by an abiotic GR mineral invites further research into the relationship between the evolution of primitive microbial metabolisms and the abiotic geochemical processes that preceded them.

**Ethics.** This work did not require ethical approval from a human subject or animal welfare committee.

**Data accessibility.** The data are provided in electronic supplementary material [76].

**Declaration of AI use.** We have not used AI-assisted technologies in creating this article.

**Authors' contributions.** O.F.: conceptualization, data curation, formal analysis, investigation, methodology, project administration, validation, visualization, writing—original draft, writing—review and editing; N.G.: investigation, visualization, writing—review and editing; G.D.: methodology, resources, software, supervision, writing—review and editing; M.J.R.: conceptualization, methodology, project administration, supervision, writing—review and editing; D.F.: conceptualization, funding acquisition, project administration, supervision, writing—review and editing; W.N.: conceptualization, funding acquisition, project administration,

resources, supervision, validation, writing—review and editing; S.D.: conceptualization, funding acquisition, investigation, project administration, resources, supervision, validation, writing—review and editing.

All authors gave final approval for publication and agreed to be held accountable for the work performed therein.

**Conflict of interest declaration.** The authors declare no conflict of interest.

**Funding.** This work received support from the French Government under the France 2030 investment plan, as part of the initiative d'Excellence d'Aix Marseille Université (grant no. A\*MIDEX -AMX-21-PEP-039) as well as a grant from the French Agence Nationale pour la Recherche (grant no. ANR-22-CE30-0035-01)

**Acknowledgements.** We thank Vasile Heresanu for performing XRD measurements, Alexandre Altié and Damien Chaudanson for SEM/TEM support, Frederic Brunel for lending us the pressure reactor, and Olivier Grauby for helpful discussions on green rust.

## References

- Jackson RB *et al.* 2021 Atmospheric methane removal: a research agenda. *Phil. Trans. R. Soc. A* **379**, 20200454. (doi:10.1098/rsta.2020.0454)
- Chistoserdova L, Vorholt JA, Thauer RK, Lidstrom ME. 1998 C1 transfer enzymes and coenzymes linking methylotrophic bacteria and methanogenic archaea. *Science (1979)* **281**, 99–102. (doi:10.1126/science.281.5373.99)
- Russell MJ, Nitschke W. 2017 Methane: fuel or exhaust at the emergence of life? *Astrobiology* **17**, 1053–1066. (doi:10.1089/ast.2016.1599)
- Kopp DA, Lippard SJ. 2002 Soluble methane monooxygenase: activation of dioxygen and methane. *Curr. Opin. Chem. Biol.* **6**, 568–576. (doi:10.1016/S1367-5931(02)00366-6)
- Nizova GV, Süß-Fink G, Shul'pin GB. 1997 Catalytic oxidation of methane to methyl hydroperoxide and other oxygenates under mild conditions. *Chem. Commun.*, 397–398. (doi:10.1039/a607765j)
- Starokon EV, Parfenov MV, Arzumanov SS, Pirutko LV, Stepanov AG, Panov GI. 2013 Oxidation of methane to methanol on the surface of FeZSM-5 zeolite. *J. Catal.* **300**, 47–54. (doi:10.1016/j.jcat.2012.12.030)
- Dummer NF *et al.* 2023 Methane oxidation to methanol. *Chem. Rev.* **123**, 6359–6411. (doi:10.1021/acs.chemrev.2c00439)
- Banerjee R, Proshlyakov Y, Lipscomb JD, Proshlyakov DA. 2015 Structure of the key species in the enzymatic oxidation of methane to methanol. *Nature* **518**, 431–434. (doi:10.1038/nature14160)
- Arney G, Domagal-Goldman SD, Meadows VS, Wolf ET, Schwieterman E, Charnay B, Claire M, Hébrard E, Trainer MG. 2016 The pale orange dot: the spectrum and habitability of hazy Archean earth. *Astrobiology* **16**, 873–899. (doi:10.1089/ast.2015.1422)
- Catling DC, Zahnle KJ. 2020 The Archean atmosphere. *Sci. Adv.* **6**, eaax1420. (doi:10.1126/sciadv.aax1420)
- Schirmermeister BE, Gugger M, Donoghue PCJ. 2015 Cyanobacteria and the great oxidation event: evidence from genes and fossils. *Palaeontology* **58**, 769–785. (doi:10.1111/pala.12178)
- Duval S, Baymann F, Schoepp-Cothenet B, Trolard F, Bourrié G, Grauby O, Branscomb E, Russell MJ, Nitschke W. 2019 Fougerite: the not so simple progenitor of the first cells. *Interface Focus* **9**, 16–20. (doi:10.1098/rsfs.2019.0063)
- Jönsson J, Sherman DM. 2008 Sorption of As(III) and As(V) to siderite, green rust (fougerite) and magnetite: implications for arsenic release in anoxic groundwaters. *Chem. Geol.* **255**, 173–181. (doi:10.1016/j.chemgeo.2008.06.036)
- Dössing LN, Dideriksen K, Stipp SLS, Frei R. 2011 Reduction of hexavalent chromium by ferrous iron: a process of chromium isotope fractionation and its relevance to natural environments. *Chem. Geol.* **285**, 157–166. (doi:10.1016/j.chemgeo.2011.04.005)
- Choi J, Batchelor B, Won C, Chung J. 2012 Nitrate reduction by green rusts modified with trace metals. *Chemosphere* **86**, 860–865. (doi:10.1016/j.chemosphere.2011.11.035)
- Etique M, Zegeye A, Grégoire B, Carteret C, Ruby C. 2014 Nitrate reduction by mixed iron(II-III) hydroxycarbonate green rust in the presence of phosphate anions: the key parameters influencing the ammonium selectivity. *Water Res.* **62**, 29–39. (doi:10.1016/j.watres.2014.05.028)
- Onoguchi A, Granata G, Haraguchi D, Hayashi H, Tokoro C. 2019 Kinetics and mechanism of selenate and selenite removal in solution by green rust-sulfate. *R. Soc. Open Sci.* **6**, 182147. (doi:10.1098/rsos.182147)
- Buessecker S, Imanaka H, Ely T, Hu R, Romaniello SJ, Cadillo-Quiroz H. 2022 Mineral-catalysed formation of marine NO and N<sub>2</sub>O on the anoxic early Earth. *Nat. Geosci.* **15**, 1056–1063. (doi:10.1038/s41561-022-01089-9)
- Usman M, Byrne JM, Chaudhary A, Orsetti S, Hanna K, Ruby C, Kappler A, Haderlein SB. 2018 Magnetite and green rust: synthesis, properties, and environmental applications of mixed-valent iron minerals. *Chem. Rev.* **118**, 3251–3304. (doi:10.1021/acs.chemrev.7b00224)
- Trolard F, Bourrié G. 2008 Geochemistry of green rusts and fougerite: a reevaluation of Fe cycle in soils. *Adv. Agronomy* **99**, 227–288. (doi:10.1016/S0065-2113(08)00405-7)
- Zegeye A *et al.* 2012 Green rust formation controls nutrient availability in a ferruginous water column. *Geology* **40**, 599–602. (doi:10.1130/G32959.1)
- Farr O, Elzinga EJ, Yee N. 2022 Effect of Ni<sup>2+</sup>, Zn<sup>2+</sup>, and Co<sup>2+</sup> on green rust transformation to magnetite. *Geochem. Trans.* **23**, 3. (doi:10.1186/s12932-022-00080-y)
- Dodd MS *et al.* 2022 Abiotic anoxic iron oxidation, formation of Archean banded iron formations, and the oxidation of early Earth. *Earth Planet. Sci. Lett.* **584**, 117469. (doi:10.1016/j.epsl.2022.117469)
- Halevy I, Alesker M, Schuster EM, Popovitz-Biro R, Feldman Y. 2017 A key role for green rust in the Precambrian oceans and the genesis of iron formations. *Nat. Geosci.* **10**, 135–139. (doi:10.1038/ngeo2878)
- Russell M. 2018 Green rust: the simple organizing 'seed' of all life? *Life* **8**, 35. (doi:10.3390/life8030035)
- Russell MJ. 2023 A self-sustaining serpentinization mega-engine feeds the fougerite nanoengines implicated in the emergence of guided metabolism. *Front. Microbiol.* **14**, 1145915. (doi:10.3389/fmicb.2023.1145915)
- Barge LM, Flores E, Baum MM, Velde DGV, Russell MJ. 2019 Redox and pH gradients drive amino acid synthesis in iron oxyhydroxide mineral systems. *Proc. Natl Acad. Sci. USA* **116**, 4828–4833. (doi:10.1073/pnas.1812098116)
- Ruby C, Géhin A, Abdelmoula M, Génin JMR, Jolivet JP. 2003 Coprecipitation of Fe(II) and Fe(III) cations in sulphated aqueous medium and formation of hydroxysulphate green rust. *Solid State Sci.* **5**, 1055–1062. (doi:10.1016/S1293-2558(03)00121-3)
- Bocher F, Géhin A, Ruby C, Ghanbaja J, Abdelmoula M, Génin JMR. 2004 Coprecipitation of Fe(II-III) hydroxycarbonate green rust stabilised by



- phosphate adsorption. *Solid State Sci.* **6**, 117–124. (doi:10.1016/j.solidstatesciences.2003.10.004)
30. Duan Z, Möller N, Greenberg J, Weare JH. 1992 The prediction of methane solubility in natural waters to high ionic strength from 0 to 250°C and from 0 to 1600 bar. *Geochim. Cosmochim. Acta* **56**, 1451–1460. (doi:10.1016/0016-7037(92)90215-5)
  31. Agnel MI, Grangeon S, Fauth F, Elkaïm E, Claret F, Roulet M, Warmont F, Tournassat C. 2020 Mechanistic and thermodynamic insights into anion exchange by green rust. *Environ. Sci. Technol.* **54**, 851–861. (doi:10.1021/acs.est.9b05632)
  32. Lee S, Wang C, Chakrapani V. 2023 Spontaneous unassisted conversion of CO<sub>2</sub> to multicarbon liquid products on green rust mineral. *ChemRxiv*. (doi:10.26434/chemrxiv-2023-bch3f-v2)
  33. Erbs M, Hansen HCB, Olsen CE. 1999 Reductive dechlorination of carbon tetrachloride using iron(II) iron(III) hydroxide sulfate (green rust). *Environ. Sci. Technol.* **33**, 307–311. (doi:10.1021/es980221t)
  34. Szécsényi Á, Li G, Gascon J, Pidko EA. 2018 Mechanistic complexity of methane oxidation with H<sub>2</sub>O<sub>2</sub> by single-site Fe/ZSM-5 catalyst. *ACS Catal.* **8**, 7961–7972. (doi:10.1021/acscatal.8b01672)
  35. Fang L, Xu L, Deng J, Gao S, Huang LZ. 2021 Induced generation of hydroxyl radicals from green rust under oxic conditions by iron-phosphate complexes. *Chem. Eng. J.* **414**, 128780. (doi:10.1016/j.cej.2021.128780)
  36. Li Z, Li M, Tan B, Du N, Zhang Q, Li C, Zhang Y, Li J, Li J. 2022 Green rust (GR) and glucose oxidase (GOX) based Fenton-like reaction: capacity of sustainable release, promoted conversion of glucose through GOX-iron and pH self-adjustment. *Environ. Res.* **208**, 112656. (doi:10.1016/j.envres.2021.112656)
  37. Hanna K, Kone T, Ruby C. 2010 Fenton-like oxidation and mineralization of phenol using synthetic Fe(II)–Fe(III) green rusts. *Environ. Sci. Pollut. Res.* **17**, 124–134. (doi:10.1007/s11356-009-0148-y)
  38. Matta R, Hanna K, Chiron S. 2008 Oxidation of phenol by green rust and hydrogen peroxide at neutral pH. *Sep. Purif. Technol.* **61**, 442–446. (doi:10.1016/j.seppur.2007.12.005)
  39. Anipitakis GP, Dionysiou DD. 2004 Radical generation by the interaction of transition metals with common oxidants. *Environ. Sci. Technol.* **38**, 3705–3712. (doi:10.1021/es035121o)
  40. Alshehri A. 2013 Methanol oxidation on transition elements oxides. PhD thesis, Cardiff University, Cardiff, UK.
  41. Rabiou AM, Yusuf IM. 2013 Industrial feasibility of direct methane conversion to hydrocarbons over Fe-based Fischer Tropsch catalyst. *J. Power Energy Eng.* **1**, 41–46. (doi:10.4236/jpee.2013.15006)
  42. Trolard F, Duval S, Nitschke W, Ménez B, Pisapia C, Ben Nacib J, Andréani M, Bourrié G. 2022 Mineralogy, geochemistry and occurrences of fougérite in a modern hydrothermal system and its implications for the origin of life. *Earth Sci. Rev.* **225**, 103910. (doi:10.1016/j.earscirev.2021.103910)
  43. Maithreepala RA, Doong RA. 2005 Enhanced dechlorination of chlorinated methanes and ethenes by chloride green rust in the presence of copper(II). *Environ. Sci. Technol.* **39**, 4082–4090. (doi:10.1021/es048428b)
  44. Choi J, Lee W. 2008 Enhanced degradation of tetrachloroethylene by green rusts with platinum. *Environ. Sci. Technol.* **42**, 3356–3362. (doi:10.1021/es702661d)
  45. O'Loughlin EJ, Burriss DR. 2022 Reduction of chlorinated ethenes by Ag- and Cu-amended green rust. *Minerals* **12**, 138. (doi:10.3390/min12020138)
  46. Yao W, Zhang J, Gu K, Li J, Qian J. 2022 Synthesis, characterization and performances of green rusts for water decontamination: a review. *Environ. Pollut.* **304**, 119205. (doi:10.1016/j.envpol.2022.119205)
  47. Huber SG, Kotte K, Schöler HF, Williams J. 2009 Natural abiotic formation of trihalomethanes in soil: results from laboratory studies and field samples. *Environ. Sci. Technol.* **43**, 4934–4939. (doi:10.1021/es8032605)
  48. Redeker KR, Kalin RM. 2012 Methyl chloride isotopic signatures from Irish forest soils and a comparison between abiotic and biogenic methyl halide soil fluxes. *Glob. Chang. Biol.* **18**, 1453–1467. (doi:10.1111/j.1365-2486.2011.02600.x)
  49. Wittmer J, Bleicher S, Ofner J, Zetzsch C. 2015 Iron(III)-induced activation of chloride from artificial sea-salt aerosol. *Environ. Chem.* **12**, 461–475. (doi:10.1071/EN14279)
  50. Bahlmann E, Keppler F, Wittmer J, Greule M, Schöler HF, Seifert R, Zetzsch C. 2019 Evidence for a major missing source in the global chloromethane budget from stable carbon isotopes. *Atmos. Chem. Phys.* **19**, 1703–1719. (doi:10.5194/acp-19-1703-2019)
  51. Sattler T *et al.* 2019 Natural formation of chloro- and bromoacetone in salt lakes of Western Australia. *Atmosphere (Basel)* **10**, 663. (doi:10.3390/atmos10110663)
  52. Trolard F, Génin J-MR, Abdelmoula M, Bourrié G, Humbert B, Herbillion A. 1997 Identification of a green rust mineral in a reductomorphic soil by Mossbauer and Raman spectroscopies. *Geochim. Cosmochim. Acta* **61**, 1107–1111. (doi:10.1016/S0016-7037(96)00381-X)
  53. Jorand F, Zegeye A, Ghanbaja J, Abdelmoula M. 2011 The formation of green rust induced by tropical river biofilm components. *Sci. Total Environ.* **409**, 2586–2596. (doi:10.1016/j.scitotenv.2011.03.030)
  54. Li Q, Fernandez RP, Hossaini R, Iglesias-Suarez F, Cuevas CA, Apel EC, Kinnison DE, Lamarque JF, Saiz-Lopez A. 2022 Reactive halogens increase the global methane lifetime and radiative forcing in the 21st century. *Nat. Commun.* **13**, 2768. (doi:10.1038/s41467-022-30456-8)
  55. Poulton SW, Canfield DE. 2011 Ferruginous conditions: a dominant feature of the ocean through Earth's history. *Elements* **7**, 107–112. (doi:10.2113/gselements.7.2.107)
  56. Thibon F, Blichert-Toft J, Tsikos H, Foden J, Albalat E, Albarede F. 2019 Dynamics of oceanic iron prior to the Great Oxygenation Event. *Earth Planet. Sci. Lett.* **506**, 360–370. (doi:10.1016/j.epsl.2018.11.016)
  57. Koeksoy E, Sundman A, Byrne JM, Lohmayer R, Planer-Friedrich B, Halevy I, Konhauser KO, Kappler A. 2019 Formation of green rust and elemental sulfur in an analogue for oxygenated ferro-euxinic transition zones of Precambrian oceans. *Geology* **47**, 211–214. (doi:10.1130/G45501.1)
  58. He H, Wu X, Xian H, Zhu J, Yang Y, Lv Y, Li Y, Konhauser KO. 2021 An abiotic source of Archean hydrogen peroxide and oxygen that pre-dates oxygenic photosynthesis. *Nat. Commun.* **12**, 611. (doi:10.1038/s41467-021-26916-2)
  59. Zhao G, Tan M, Wu B, Zheng X, Xiong R, Chen B, Kappler A, Chu C. 2023 Redox oscillations activate thermodynamically stable iron minerals for enhanced reactive oxygen species production. *Environ. Sci. Technol.* **57**, 8628–8637. (doi:10.1021/acs.est.3c02302)
  60. He H *et al.* 2023 A mineral-based origin of Earth's initial hydrogen peroxide and molecular oxygen. *Proc. Natl Acad. Sci. USA* **120**, e2221984120. (doi:10.1073/pnas.2221984120)
  61. Ernst L, Barayeu U, Hädeler J, Dick TP, Klatt JM, Keppler F, Rebelein JG. 2023 Methane formation driven by light and heat prior to the origin of life and beyond. *Nat. Commun.* **14**, 4364. (doi:10.1038/s41467-023-39917-0)
  62. Huang Q, Jiang S-Y, Pi D-H, Konhauser KO, Wen X-P, Lu L-Y, Yan H. 2023 Thermochemical oxidation of methane by manganese oxides in hydrothermal sediments. *Commun. Earth Environ.* **4**, 224. (doi:10.1038/s43247-023-00891-6)
  63. Nitschke W *et al.* 2022 Aqueous electrochemistry: the toolbox for life's emergence from redox disequilibria. *Electrochem. Sci. Adv.* **3**, e2100192. (doi:10.1002/elsa.202100192)
  64. Ooka H, McGlynn SE, Nakamura R. 2019 Electrochemistry at deep-sea hydrothermal vents: utilization of the thermodynamic driving force towards the autotrophic origin of life. *ChemElectroChem* **6**, 1316–1323. (doi:10.1002/celec.201801432)
  65. Lee S, Wang C, Chakrapani V. 2023 Spontaneous unassisted conversion of CO<sub>2</sub> to multicarbon (≥ C<sub>2</sub>) liquid products on green rust mineral. *ChemRxiv*. (doi:10.26434/chemrxiv-2023-bch3f)
  66. Wong ML, Charnay BD, Gao P, Yung YL, Russell MJ. 2017 Nitrogen oxides in early Earth's atmosphere as electron acceptors for life's emergence. *Astrobiology* **17**, 975–983. (doi:10.1089/ast.2016.1473)
  67. Ducluzeau AL, van Lis R, Duval S, Schoepp-Cothenet B, Russell MJ, Nitschke W. 2009 Was nitric oxide the first deep electron sink? *Trends Biochem. Sci.* **34**, 9–15. (doi:10.1016/j.tibs.2008.10.005)
  68. Barge LM *et al.* 2022 Prebiotic reactions in a Mars analog iron mineral system: effects of nitrate, nitrite, and ammonia on amino acid formation. *Geochim. Cosmochim. Acta* **336**, 469–479. (doi:10.1016/j.gca.2022.08.038)



69. Guilbaud R, Poulton SW, Butterfield NJ, Zhu M, Shields-Zhou GA. 2015 A global transition to ferruginous conditions in the early Neoproterozoic oceans. *Nat. Geosci.* **8**, 466–470. (doi:10.1038/NGEO2434)
70. Jaziri AY, Charnay B, Selsis F, Leconte J, Lefèvre F. 2022 Dynamics of the great oxidation event from a 3D photochemical-climate model. *Clim. Past* **18**, 2421–2447. (doi:10.5194/cp-18-2421-2022)
71. Leung M, Schwieterman EW, Parenteau MN, Faucher TJ. 2022 Alternative methylated biosignatures. I. Methyl bromide, a capstone biosignature. *Astrophys. J.* **938**, 6. (doi:10.3847/1538-4357/ac8799)
72. Russell MJ, Nitschke W, Branscomb E. 2013 The inevitable journey to being. *Phil. Trans. R. Soc. B* **368**, 20120254. (doi:10.1098/rstb.2012.0254)
73. Branscomb E, Russell MJ. 2018 Frankenstein or a submarine alkaline vent: who is responsible for abiogenesis? Part 2. As life is now, so it must have been in the beginning. *Bioessays* **40**, 1700182. (doi:10.1002/bies.201700182)
74. Nitschke W, McGlynn SE, Milner-White EJ, Russell MJ. 2013 On the antiquity of metalloenzymes and their substrates in bioenergetics. *Biochim. Biophys. Acta Bioenerg.* **1827**, 871–881. (doi:10.1016/j.bbabi.2013.02.008)
75. Helmbrecht V, Weingart M, Klein F, Braun D, Orsi WD. 2022 White and green rust chimneys accumulate RNA in a ferruginous chemical garden. (<https://arxiv.org/abs/2212.02793>)
76. Farr O, Gaudu N, Danger G, Russell MJ, Ferry D, Nitschke W, Duval S. 2023 Methanol on the rocks: green rust transformation promotes the oxidation of methane. Figshare. (doi:10.6084/m9.figshare.c.6825590)